Author Manuscript

Author Manuscript

Author Manuscript

Author Manuscript

HHS Public Access

Author manuscript

J Photochem Photobiol B. Author manuscript; available in PMC 2015 June 17.

Published in final edited form as:

J Photochem Photobiol B. 2005 June 1; 79(3): 231–241. doi:10.1016/j.jphotobiol.2004.09.013.

Determination of the distribution of light, optical properties, drug concentration, and tissue oxygenation in-vivo in human prostate during motexafin lutetium-mediated photodynamic therapy

Timothy C. Zhu, **Jarod C. Finlay**, and **Stephen M. Hahn***

Department of Radiation Oncology, Hospital of the University of Pennsylvania, 3400 Spruce Street, Philadelphia, PA 19104-4283, USA

Abstract

It is desirable to quantify the distribution of the light fluence rate, the optical properties, the drug concentration, and the tissue oxygenation for photodynamic therapy (PDT) of prostate cancer. We have developed an integrated system to determine these quantities before and after PDT treatment using motorized probes. The optical properties (absorption (μ_a), transport scattering (μ_s'), and effective attenuation (μ_{eff}) coefficients) of cancerous human prostate were measured in-vivo using interstitial isotropic detectors. Measurements were made at 732 nm before and after motexafin lutetium (MLu) mediated PDT at different locations along each catheter. The light fluence rate distribution was also measured along the catheters during PDT. Diffuse absorption spectroscopy measurement using a white light source allows extrapolation of the distribution of oxygen saturation (StO_2), total blood volume ($[Hb]_t$), and MLu concentration. The distribution of drug concentration was also studied using fluorescence from a single optical fiber, and was found to be in good agreement with the values determined by absorption spectroscopy. This study shows significant inter- and intra-prostatic variations in the tissue optical properties and MLu drug distribution, suggesting that a real-time dosimetry measurement and feedback system for monitoring these values during treatment should be considered in future PDT studies.

Keywords

PDT; In-vivo; Optical properties; Prostate; MLu; Motexafin lutetium

1. Introduction

Prostate adenocarcinoma is the most common malignancy in men. In 2003, it was estimated that 220,900 cases of prostate adenocarcinoma were diagnosed in the United States [1]. Although the availability of serum prostate-specific antigen (PSA) measurement as a screening tool has resulted in earlier detection of the disease [2], prostate cancer still accounted for 28,900 deaths in 2003 [1].

© 2004 Elsevier B.V. All rights reserved.

*Corresponding author. Tel.: +1 215 662 7296; fax: +1 215 349 5445. hahn@xrt.upenn.edu (S.M. Hahn).

Author Manuscript Author Manuscript Author Manuscript Author Manuscript

Photodynamic therapy (PDT) is an emerging treatment modality based on the interaction of light, a photosensitizing drug, and oxygen [3]. PDT has been a proposed treatment for a variety of malignancies and premalignant conditions. PDT has been approved by the US Food and Drug Administration for the treatment of microinvasive lung cancer, obstructing lung cancer, and obstructing esophageal cancer. The prostate gland is an organ that appears to be a good target for interstitial PDT. Tumors of the prostate are often confined to the prostate itself and brachytherapy techniques used for the placement of radioactive seed implants can be adapted for the placement of interstitial optical fibers [4]. Several preclinical studies have evaluated the feasibility of delivering PDT to the prostate via this interstitial approach [5–10]. A trial of interstitial prostate PDT in humans has been reported [11]. Nathan et al. treated 14 men with locally recurrent prostate cancer using meso-tetrahydroxyphenyl chlorin (mTHPC)-mediated interstitial PDT. The light treatment was directed against regions from which biopsies showed cancer or which were suspicious on imaging studies.

Motexafin lutetium (MLu) is a water-soluble second generation synthetic photoactive drug that has a Q-band absorption peak at 732 nm [12,13]. Based on a feasibility and toxicity study in a canine prostate model [9], we have started a phase I study of MLu-mediated PDT for prostate cancer [14]. In the canine study, comprehensive treatment of the prostate gland was achieved with MLu-mediated PDT using an interstitial approach. The development of this light delivery technique has necessitated an improved understanding of PDT dosimetry, critical for determining the efficacy of the PDT treatment.

Explicit PDT dosimetry includes quantifying the light and tissue optical properties, the drug concentration, and the tissue oxygenation. The light fluence (expressed in J/cm^2) is a measure of light energy imparted to tissue. The total fluence in tissues is a function not only of the incident light delivered by the laser but also of scattered light. Often clinical PDT treatments are prescribed in terms of the incident light delivered from the laser rather than the total fluence of light the tissues receive which is a combination of scattered and incident light. Dosimetry systems using isotropic light detectors have been developed to measure both incident and scattered light [15,16]. These systems allow us to measure and therefore prescribe a consistent total fluence to the tissues.

Several investigators have attempted to characterize the optical properties of prostate tissue in animals [17– 19] and in humans [20–22] to more reliably predict the in vivo light distribution. Using diffusion theory for a point source, the absorption and transport scattering coefficients of a particular tissue can be determined, yielding the effective attenuation coefficient, which provides a measure of light penetration in that tissue [18]. This measurement is a critical factor in planning interstitial light source placement. To include the drug concentration in the evaluation of PDT efficacy, in situ measurements of photosensitizer fluorescence emission are made in the prostate using a single optical fiber, originally developed for surface application by Diamond et al. [23]. We have modified their technique by replacing the flat cut fiber with a side fire fiber to introduce light interstitially to the target tissue more efficiently. It has also been shown that one can determine MLu concentration using diffuse absorption spectra [24]. The MLu concentration in prostate tissue can be determined using a slightly modified technique via an interstitial approach

Author Manuscript Author Manuscript Author Manuscript Author Manuscript

[25]. The MLu tissue concentrations determined from absorption spectra can be compared to those obtained using fluorescence spectra. Using the same diffuse absorption spectra, it is also possible to determine the concentrations of deoxyhemoglobin ([Hb]) and oxyhemoglobin ($[HbO_2]$) [24–27]. To determine the tissue oxygenation, the oxygen saturation ratio $StO_2 = [HbO_2]/([Hb] + [HbO_2])$ and total hemoglobin concentration $[Hb]_t = [Hb] + [HbO_2]$ can be calculated.

In this study, we review our preliminary observations measuring the interstitial distribution of light fluence rate, optical properties, tissue MLu concentration, and tissue oxygenation in two patients with prostate cancer. Measurements were made before and after PDT treatment in which the entire prostate was treated. Intraprostatic as well as interprostatic differences were evaluated.

2. Materials and methods

2.1. Patient selection, surgical and PDT procedure

A Phase I clinical trial of PDT with MLu in patients with locally recurrent prostate carcinoma was initiated at the University of Pennsylvania in 1999. The protocol was approved by the Institutional Review board of the University of Pennsylvania, the Clinical Trials and Scientific Monitoring Committee (CTSRMC) of the University of Pennsylvania Cancer Center, and the Cancer Therapy Evaluation Program (CTEP) of the National Cancer Institute. Each patient who signed the informed consent document underwent an evaluation, which included an MRI of the prostate, bone scan, laboratory studies including PSA, and a urological evaluation. Approximately two weeks prior to the scheduled treatment a transrectal ultrasound (TRUS) was performed for treatment planning. A urologist drew the target volume (the prostate) on each slice of the ultrasound images. These images were spaced 0.5 cm apart and were scanned with the same ultrasound unit used for treatment. A built-in template with a 0.5-cm grid projected the locations of possible light sources relative to the prostate. A treatment plan was then prepared to determine the location and length of light sources. Cylindrical diffusing fibers (CDF's) with active lengths 1, 2, 3, 4, and 5 cm were used. The sources were spaced one centimeter apart and the light power per unit length was the same for all CDF's. The length of a light source at a particular position was selected to cover the full length of the prostate. In the final plan, the prostate was divided into four quadrants. Four isotropic detectors were used, each placed in the center of one quadrant. A fifth isotropic detector was placed in a urethral catheter to monitor the light fluence in the urethra.

The patients were anesthetized in the operating room with general anesthesia to minimize patient movement during the procedure. Transrectal ultrasound-guided biopsies for MLu measurements were obtained prior to light delivery. The same ultrasound unit used to perform the pretreatment TRUS was used to guide needle placement in the operating room. A template was attached to the ultrasound unit and was matched to the 0.5-cm grid used for treatment planning. Four detector catheters (one for each quadrant) were inserted into the prostate. These detectors were kept in place during the entire light delivery period. The pre-planned treatment catheters for light sources were then inserted 0.5 or 0.7 cm away from the detector catheters. These source catheters were used for light delivery as well as optical

Author Manuscript Author Manuscript Author Manuscript Author Manuscript

properties and absorption spectra measurements. The optical properties and absorption spectra of the prostate in each quadrant were then measured before light delivery using these existing detectors. A point light source was inserted into one source catheter. Fluorescence measurements were made through the detector catheter in each quadrant using a single optical fiber acting as both a light source and a detector. The fiber introduced 460 nm light and collected fluorescence light above 700 nm at right angles from the optical axis of the beveled fiber tip. The distribution measurements of optical properties, absorption spectra and fluorescence were completed in approximately 10 min. Light delivery was then performed one quadrant at a time by inserting the CDFs into the source catheters. The treatment time for each quadrant was dependent on the detector reading in that quadrant. The light fluence rate distributions were measured during PDT along the catheters. Cumulative fluences of 50 and 100 J/cm^2 were delivered to patients 12 and 13, respectively. After light delivery, the optical properties and absorption and fluorescence of the prostate in all four quadrants were measured again. The light sources and detectors were then removed and post-treatment biopsies were performed.

2.2. Computer controlled step motors

Two step motors were used to control the movement of the light source and the isotropic detector during optical property measurements (see Fig. 1(a)). Each step motor and translational stage had a maximum range of 20 cm and a maximum speed of 12.5 mm/s. The step motor produced 400 pulses per rotation, which translated to a resolution of 0.0025 mm. Control software was developed to integrate the movement of the step motor with data acquisition of isotropic detectors as well as the spectrometer for fluorescence and absorption spectra measurements. For the integrated system, the positioning accuracy was 0.1 mm. The data acquisition system was programmed to acquire data every 0.05 mm of detector movement.

To determine the relative position between the light source and the isotropic detector for optical properties or absorption spectra measurements, software was developed to automatically reset the position of the peak fluence rate as the zero position. This point corresponded to the point with the shortest distance between the line defined by the detector catheter and the point source. A similar scan was used for a white light source to determine the relative distances between the light source and the locations where the diffuse absorption spectra were taken, typically at x = −0.4, −0.2, 0, 0.2, 0.4, 0.6, 0.8, 1.0, 1.2, 1.4, and 1.6 cm. The position of the light source was defined as the distance of the source from the tip of catheter, intended to be placed at the apex of the prostate under ultrasound guidance.

2.3. Measurement of optical properties at the treatment wavelength

The transport scattering (μ_s') and absorption (μ_a) coefficients characterize the scattering and absorption properties of tissue. Within the diffusion approximation, the light fluence rate φ at a distance r from a point source of source strength, S, can be expressed as [28]

$$\phi = \frac{S \cdot \mu_{\text{eff}}^2}{4\pi r \cdot \mu_a} e^{-\mu_{\text{eff}} \cdot r} = \frac{S \cdot 3\mu_s'}{4\pi r} e^{-\mu_{\text{eff}} \cdot r}; \quad (1)$$

Author Manuscript Author Manuscript Author Manuscript Author Manuscript

where S is the strength of the point source; $\varphi(r)$ is the fluence rate at position r; $\mu_{\text{eff}}=\sqrt{3\cdot\mu_a\cdot\mu_s'}$ is the effective attenuation coefficient in tissues and is applicable for a wider range of μ_a and μ_s' combinations than the traditional definition of $\mu_{\text{eff}}=\sqrt{3\cdot\mu_a\cdot(\mu_s'+\mu_a)}$ [29]. $r=\sqrt{x^2+h^2}$, where x and h are the parallel and perpendicular distance from the center of the point source (see Fig. 1(b)). The two free parameters (μ_a and μ_s') are inherently separable in that for a point source with a given source strength, the magnitude of the fluence rate near the light source ($x = 0$) is determined by μ_s' only and the slope of the spatial decay of the light fluence rate is determined by μ_{eff} only.

In theory, measurements of φ at two different distances r from the point source with source strength S are sufficient to determine both μ_a and μ_s'. Measurements at multiple sites allow evaluating the variation of these optical characteristics within the prostate volume. Since Eq. (1) is a non-linear equation of two free parameters μ_a and μ_s', we used the differential evolution algorithm developed by Storn et al. [30]. This algorithm is simple, and converges faster and is more robust than adaptive simulated annealing or the annealed Nelder and Mead approach [30]. We modified the algorithm to require that all free parameters (μ_a and μ_s' in this case) are positive [31]. The deviations between measurement and fit are represented by standard deviation, $\sum_{i=1}^{n}\sqrt{(\text{fit}_i-\text{meas}_i)^2/(n-1)}$, where n is the number of data points involved in the fit.

2.4. Calibration of the isotropic detector

Isotropic detectors described by Marijnissen and Star [32] were used as detectors in this study. Each isotropic detector was made of an optical fiber with a spherical tip made of TiO_2 (a scattering material). The isotropic detectors were made by Rare Earth Medical (now CardioFocus, Norton, MA) and had an isotropy of better than ±30% from any direction except for angles within 30° of the optical fiber attachment point. Each detector fiber was connected to a photodiode via a SMA connector. The measured photovoltage (V) from the isotropic detector was converted to light fluence rate using:

$$\phi=a(V-b), \quad (2)$$

where a is the conversion factor and b characterizes the leakage of the photodiode. This calibration was performed under collimated 732-nm laser light in air. When the isotropic detector was used to measure fluence rate in tissue (or in a liquid optical phantom), a tissue (or water) correction factor of 2.0 was used [32]. In our case, the 1 mm inner diameter catheter is filled with air, but the detector tissue correction factor is still 2.0 as if the air is replaced by the outer most medium (tissue). The calibration of the isotropic detectors was checked to be accurate to within 5% using an integrating sphere before each individual measurement.

A 12-channel light dosimetry system developed in the Department of Radiation Oncology at the University of Pennsylvania was used for all in situ dosimetry measurements. Five

Author Manuscript Author Manuscript Author Manuscript Author Manuscript

different isotropic detectors were used and the conversion factors were a = 129–161 and a = 63–72 mW/cm^2/V for the four isotropic detectors with 0.5 mm scattering tips and the isotropic detector with 1 mm scattering tip used in the urethra, respectively. For all isotropic detectors, b was found to be 0.020 V. The response was found to be linear over the light fluence rate range (0–1200 mW/cm^2) to within 5%.

2.5. Absorption and fluorescence spectroscopy measurements

To obtain absorption spectra, a method similar to the optical property measurement described above was used. In this case, the laser and photodiode detector were replaced with a white light source and a spectrograph, respectively. To calibrate the detector, the detection fiber and source fiber were both placed in the integrating sphere, and a reference spectrum was obtained by the CCD. The fluence rate measured at each wavelength was related to the source power at that wavelength by a constant factor determined by the geometry of the integrating sphere. This factor was calculated based on independent measurements at three wavelengths using a calibrated detector. With this calibration, the detector measures the ratio of fluence rate to source power. The fluence rate spectra between 650 and 800 nm were fit using a nonlinear fitting algorithm under the assumption that the reduced scattering spectrum had the form $\mu_s' = A\lambda^{-b}$, where λ is expressed in nm. The free parameters in the fit were A, b, and the absorption coefficients at 8 selected wavelengths. Once A and b were determined by this fit, the absorption coefficients at the remaining wavelengths were determined by a second fit in which the value of μ_s' was fixed at its predetermined value for each wavelength [25]. The measurement uncertainty of the absorption spectra has been examined in optical phantoms made of intralipid, MLu, and black ink, each with known absorption spectra. A comparison between the absorption spectra obtained by our measurement and analysis method and the absorption spectrum reconstructed from individual spectra of the phantom components shows that our algorithm can reconstruct μ_a with an uncertainty of approximately 5% for the wavelength range where absorption is appreciable, in the phantom case between 650–800 nm (data not shown).

Fluorescence spectra were acquired using an optical fiber with a beveled tip, which emits and collects light at right angles to its optical axis. Excitation light was provided by a 460-nm light-emitting diode (LED), and passed through a dichroic beamsplitter, which directed the fluorescence collected by the same fiber back into the spectrograph.

Both the absorption and fluorescence spectra were analyzed using the singular value decomposition fitting algorithm developed by Finlay et al. [33] to determine the contributions to the spectra of known absorbers or fluorophores. In addition to the spectra of known components, the basis set included a 61-term, exponentially weighted Fourier series designed to account for the presence of unknown absorbers or fluorophores [33]. In the case of absorption spectra, the known spectra were those of oxy- and deoxyhemoglobin, MLu and water. Because the absorption coefficient at each wavelength is determined absolutely, the absolute concentrations of the various absorbers can be determined quantitatively from their contributions to the complete absorption spectrum.

Author Manuscript Author Manuscript Author Manuscript Author Manuscript

In the fluorescence case the basis spectra were the fluorescence of MLu and the background fluorescence originating in the catheter. The fitting algorithm allows the separation of these two components, allowing us to determine an MLu contribution free from background contamination. The MLu fluorescence was normalized by dividing by the catheter background to account for variations in lamp output. A single conversion factor of 12.9 mg/kg between normalized fluorescence signal at the peak wavelength (unitless) and MLu concentration (mg/kg) was established by comparing the signal obtained in one prostate in vivo to the MLu concentration at the same position determined by absorption spectroscopy. Once this factor was determined, the fluorescence could be analyzed independent of absorption measurements in each quadrant.

2.6. Photodynamic therapy and in-vivo light measurements

MLu (Pharmacyclics, Inc., Sunnyvale, CA) was administered at a dose of 2 mg/kg intravenously 3 h prior to light administration [12,13]. This drug-light interval was chosen because preclinical studies in other model systems demonstrated the greatest antitumor efficacy with this timing [12,34]. A 15-W diode laser, model 730 (Diomed, Ltd., Cambridge, United Kingdom) was used as the 732 nm light source.

Interstitial CDFs were placed in the gland using a template with evenly spaced holes, which was attached to the TRUS unit. For each light source, a 17-gauge plastic catheter (Flexi-needle from Best Industries, Inc., Springfield, VA) containing a metal trocar was placed through the template and into the prostate. The trocar was removed and replaced with the light diffuser.

The light energy delivered was prescribed based on in situ measured light fluence. Each patient received a light fluence between 50–100 J/cm^2. The maximum unit length source strength in any one fiber was limited to 150 mW/cm. Measurements were taken at the above mentioned distances from the light source before and after light treatment in the four quadrants of each prostate. The light sources were moved along the catheter in several locations to quantify the variation of optical properties in the prostate gland along the catheter.

3. Results

Table 1 summarizes the treatment parameters and the measurements done for the two patients. We have made four types of measurements: (1) Distribution of light fluence rate; (2) Distribution of optical properties at treatment wavelength; (3) Distribution of absorption spectra; (4) Distribution of fluorescence spectra. Tissue oxygenation and MLu concentration can be extracted from absorption spectra in vivo. MLu concentration in vivo is also extracted from the fluorescence spectra.

3.1. Distribution of fluence rate

Fig. 2 shows the light fluence rate measured in three quadrants during PDT treatment of patient 13. Three curves are shown. The first, labeled ‘RUQ’ was taken by a detector in the right upper quadrant of the prostate during interstitial illumination of that quadrant. The light fluence rate for RUQ (solid line) between 1.5 and 2.5 cm was about 5 times as high as the

Author Manuscript Author Manuscript Author Manuscript Author Manuscript

rest of region (e.g., between 3 and 4.5 cm). This was caused by the loading pattern of the light sources, in which two 1-cm CDF's were placed at the apex of the prostate. The second curve, labeled 'LLQ' shows the light fluence rate that was measured in the left lower quadrant during illumination of the left upper quadrant, and demonstrates the possible extent of light spread between quadrants. The third curve labeled 'RLQ' shows light fluence rate that was taken in the right lower quadrant during treatment of that quadrant. The symbols correspond to the predicted light fluence rate from a point source with source strength of 35 mW based on the optical properties measured along the detector catheter. (The use of a cylindrical theoretical model is not feasible due to the varying optical properties along the catheters, thus point sources are used.) The corresponding loading patterns of CDF's ('o') and the locations of the detector ('x') are shown in the insert. The number next to each source channel indicates the length in cm of the corresponding CDF. All linear light sources started from the apex of the prostate ($z = 0$ cm).

We did not measure significant light fluence rate in urethra for the 12 patients treated so far.

3.2. Optical properties at treatment wavelength

A typical profile scan from a point source is shown in Fig. 3. The data were fitted using Eq. (1) to obtain the optical properties. The optical properties derived from both patients are shown in Fig. 4. These data show the variation of measured absorption coefficients and effective absorption coefficient vs. positions along the catheters in the prostate gland of patient #12 (a and b) and patient #13 (c and d). Due to time constraints we did not measure LUQ after PDT for patient #12. We did not get any results (before and after PDT) for LLQ of patient #12 and #13 due to bleeding. The effective attenuation coefficients varied between 1.9 and 6.3 cm^{-1} while the absorption coefficients varied between 0.1 and 1.6 cm^{-1} . As a result of the heterogeneity of optical properties, the light fluence rates per unit source strength at 0.5 cm from the point source varied between 0.2 and 0.6 cm^{-2} between the two patients.

3.3. Absorption spectra

A typical absorption spectrum acquired in vivo is shown in Fig. 5(a), along with the components of the spectrum as determined by linear fitting. The dominant absorbers in the wavelength region of our measurement are hemoglobin in its oxygenated and deoxygenated forms, MLu, and, to a lesser extent, water. In the cases presented here, the contribution of the Fourier synthesis was smaller than the contributions of known absorbers, indicating that the majority of absorption in tissue was accurately accounted for by our basis set. From the contributions of oxy- and deoxyhemoglobin to the measured absorption spectrum, we determined the total hemoglobin concentration $[Hb]_t$, the sensitizer concentration [MLu], and the hemoglobin oxygen saturation StO_2, given by

$$StO_2 = [HbO_2]/([Hb]+[HbO_2]). \quad (3)$$

The values of these three parameters as functions of position within a typical prostate quadrant (RUQ, patient 13), are plotted in Fig. 6(a). The concentration of MLu is given in

Author Manuscript Author Manuscript Author Manuscript Author Manuscript

ng mg^{-1} and has been scaled by a factor of 10 for comparison with the hemoglobin concentration and saturation.

3.4. Fluorescence spectra

The concentration of MLu via its intrinsic fluorescence emission was also measured around 750 nm. A typical fluorescence spectrum is shown in Fig. 5(b). The singular value decomposition fitting algorithm is able to separate the component arising from the background fluorescence of the catheter and fiber assembly (labeled 'Bkgnd') from the MLu component. The small amplitude of the Fourier component indicates that the fluorescence is dominated by these two contributions. The background fluorescence provides a measure of the lamp intensity, and is used to normalize the MLu fluorescence. The MLu distribution determined by fluorescence spectroscopy is overlaid on the corresponding distribution determined by absorption spectroscopy in Fig. 6(b). The spatial distribution of MLu determined by the two methods is similar.

4. Discussion

The main objective of this work was to demonstrate the feasibility of measuring the distribution of important dosimetric parameters for PDT in vivo, namely the tissue optical properties, tissue concentration of drug, and tissue oxygenation. Measurements were made before, during and after PDT. Differences within and between patients were also evaluated.

4.1. Distribution of light fluence rate in vivo

Our data show that there is heterogeneity of light fluence in different regions of the prostate (Fig. 2). The data also show that light delivery to one quadrant of the prostate may lead to the delivery of measurable light fluence to other regions of the prostate. For the region of high fluence rate, there were three CDFs contributing to light fluence rate, due to the contributions from the two 1-cm long CDFs and the one 4-cm long CDF. For the region of low fluence rate, only the 4-cm long linear fiber was contributing to the light fluence rate. A similar explanation can also be used for the fluence rate distribution in the LLQ. The light fluence rate for the RLQ was much larger than that for the RUQ, which can be explained by differences in optical properties. In the RLQ, two similar length CDF's were used (3 and 4 cm). If the tissue optical properties were uniform along the catheter, the profile would have been uniform. However, the profile of light fluence rate is not uniform because the optical properties change along the catheter. The predicted light fluence rate for a 35 mW source based on measured optical properties (μ_a and μ_{eff}) is indicated by symbols. The similarity in shape between the measured and the predicted light fluence rate indicates the variation of light fluence rate was due to the variation of optical properties.

4.2. Distribution of optical properties at treatment wavelength

Fig. 3 shows a typical example of measured fluence rate per source strength from a point source. The measured profile usually contains 800 data points at 0.05 mm steps. The fitting assumes that the distance *h* between the source and detector catheter is also a free variable, which is allowed to vary up to 0.2 cm from the known separation determined from the template positions. We used the same method to obtain the absorption spectra from a white

Author Manuscript Author Manuscript Author Manuscript Author Manuscript

light source using a somewhat longer step size (0.2 cm) in the range of −0.4 to 1.6 cm relative to the point source.

The intra-prostatic tissue heterogeneity of the optical properties at 732 nm is demonstrated in Fig. 4. For the same patient, the effective attenuation coefficient, μ_{eff}, varied by up to 3 times between different quadrants of the same prostate (Fig. 4(d)). This large variation of optical properties resulted in a large difference in light fluence rate between the right upper quadrant (RUQ) and the right lower quadrant (RLQ) (see Fig. 2). Within the same quadrant of a prostate, μ_{eff} can change substantially as well. Since each CDF has uniform light strength along the catheter, the variation of optical properties can result in large variation of light fluence rate along the catheter, as demonstrated by the case of the RLQ. Since our model assumes the optical properties of the medium to be homogeneous, the measured optical properties has limitation in that it should be an average of tissue optical properties within the maximum distance between the source and the detector, typically 2 cm (see Fig. 3).

The measurement standard deviation of μ_a, μ_s' and μ_{eff} is 7%, 20%, and 5%, respectively, when h is optimized in the fitting [35]. Details of the error analysis are included in [35].

Since our model assumes infinite medium, we make sure that the measurement points are at least 1 cm away from the boundaries of prostate to minimize the boundary effect. The starting position of the point source is moved 1 cm from the end of the catheter before optical properties measurement. The reduction of the light fluence rate at the tissue boundary has been characterized in a solid prostate phantom to be less than 2% at 1 cm from the boundary at 732 nm for the range of optical properties used in the study [36].

We have demonstrated in canine prostate that the absorption coefficient at 732 nm is approximately proportional to the tissue concentration of MLu [19]. This linear relationship is assumed to hold for human prostate as well. Since μ_a varied by up to 2.5 times along some catheters (Fig. 4(c), RUQ, after PDT), the tissue concentration of MLu should vary by the same magnitude along the catheter. This is consistent with the distribution of MLu concentration measured by absorption spectra and fluorescence in the same location (see Fig. 6(b)).

4.3. Distribution of absorption and fluorescence spectrum

Fig. 5(a) illustrates how one can extract the concentrations of oxyhemoglobin (HbO_2), deoxyhemoglobin (Hb), and MLu from the measured absorption spectrum. Because the absorption spectrum is determined by fitting data using Eq. (1) at each wavelength independently without the knowledge of the known spectral components [25], and because the sum of known components accurately fits the extracted spectrum with little absorption accounted for by the Fourier components, we are very confident of extracted MLu, HbO_2 and Hb concentrations. Since the average optical penetration depth ($\delta = 1/\mu_{eff}$) at 732 nm is about 0.4 cm in human prostate and the separation between the detector and the light source (0.5–1.5 cm) is generally larger than δ, the extracted quantities reflect a macroscopic average in a tissue dimension of 0.5–1.5 cm, depending on the separation between the detector and the light source. Fig. 5(b) shows the corresponding analysis of a typical

Author Manuscript Author Manuscript Author Manuscript Author Manuscript

fluorescence spectrum. The MLu concentration obtained from each spectrum is normalized to the background signal and therefore the measured MLu concentration is insensitive to variations in lamp intensity and fiber coupling efficiency. The inherent absorption by tissue is much greater at the excitation wavelength (460 nm) than the wavelengths over which we measure absorption spectra. The generation of fluorescence is therefore confined to a smaller region of tissue than that sampled by the absorption spectra measurement.

Fig. 6 illustrates the variation in total hemoglobin concentration, hemoglobin saturation, and MLu concentration within one quadrant of a typical prostate. The variation in measured $[Hb]_t$ and [MLu] likely result from variations in vascular density or perfusion, limiting the supply of drug and blood to some regions of the tissue. The agreement in the shape of the distributions of MLu determined by absorption and fluorescence spectroscopy demonstrates the ability of both methods to give quantitative information concerning the distribution of drug in vivo. While the two methods give similar information, each has its advantages. The absorption spectra measurement gives not only the drug distribution but hemodynamic information as well. The fluorescence measurement, on the other hand, samples a much smaller volume of tissue than the absorption spectra measurement, and samples many more points than is practical for absorption spectra measurements, allowing a higher-resolution map of the spatial drug distribution.

Table 1 shows the variation of optical properties before and after PDT. For patient 12, we have observed substantial reduction of MLu tissue concentration after PDT treatment, presumably due to photobleaching. A smaller reduction of MLu tissue concentration was observed for patient 13. The absorption coefficient, which has been shown to be approximately linear to MLu tissue concentration, also decreased after PDT treatment, more for patient 12 than for patient 13. The effective attenuation coefficient also varied after PDT, although the magnitude of the change was generally much smaller.

5. Conclusions

We have demonstrated inter- and intra-prostate variation of optical properties and MLu tissue concentration. The variation of optical properties can be used to explain the observed variation of light fluence rate. We observed that the optical penetration depth varied between 0.15-0.5 cm for 732 nm light within one prostate. The tissue concentration of MLu varied between 1.1 and 8 ng/mg within one prostate. These studies confirm substantial inter-organ and intra-organ variations in optical properties and drug concentration in the prostates. Given this heterogeneity, a real-time dosimetry measurement and feedback system for monitoring light fluences during treatment should be considered for interstitial prostate PDT studies.

Acknowledgement

This work is supported by a grant from National Institute of Health (NIH), R21 CA88064-01 and P01 CA87971-01, and Department of Defense (DOD), DAMD1703-1-0132.

Author Manuscript Author Manuscript Author Manuscript Author Manuscript

References

1. Jemal A, Murray T, Samuels A, Ghafoor A, Ward E, Thun MJ. Cancer statistics 2003. CA - A Cancer Journal for Clinicians. 2003; 53:5–26. [PubMed: 12568441]
2. Catalona WJ. Screening for early detection. Lancet. 1996; 347:883–884. [PubMed: 8622399]
3. Dougherty TJ, Gomer DJ, Henderson BW, et al. Photodynamic therapy. J. Natl. Cancer. Inst. 1998; 90:889–905. [PubMed: 9637138]
4. D'Amico AV. Role of interstitial radiotherapy in the management of clinically organ-confined prostate cancer: the jury is still out. J. Clin. Oncol. 1996; 14:304–315. [PubMed: 8558212]
5. Lee LK, Whitehurst C, Chen Q, Pantelides ML, Hetzel FW, Moore JV. Interstitial photodynamic therapy in the canine prostate. Br. J. Urol. 1997; 80:898–902. [PubMed: 9439405]
6. Chang SC, Buonaccorsi G, MacRobert A, Bown SG. Interstitial photodynamic therapy of the canine prostate using mesotetra- (m-hydroxyphenyl) chlorin. Int. J. Cancer. 1996; 67:555–562. [PubMed: 8759616]
7. Chang SC, Buonaccorsi G, MacRobert A, Bown SG. Interstitial photodynamic therapy of the canine prostate with disulfonated aluminum phthalocyanine and 5-aminolevulinic acid-induced protoporphyrin IX. Prostate. 1997; 32:89–98. [PubMed: 9215396]
8. Selman SH, Keck RW, Hampton JA. Transperineal photodynamic ablation of the canine prostate. J. Urol. 1996; 156:258–260. [PubMed: 8648818]
9. Hsi RA, Kapatkin A, Strandberg J, Zhu T, Vulcan T, Solonenko M, Rodriguez C, Chang J, Saunders M, Mason N, Hahn S. Photodynamic therapy in the canine prostate using motexafin lutetium. Clin. Cancer Res. 2001; 7:651–660. [PubMed: 11297261]
10. Chen Q, Huang Z, Luck D, Beckers J, Brun PH, Wilson BC, Scherz A, Salomon Y, Hetzel FW. Preclinical studies in normal canine prostate of a novel palladium-bacteriopheophorbide (WST09) photosensitizer for photodynamic therapy of prostate cancers. Photochem. Photobiol. 2002; 76(4): 438–445. [PubMed: 12405153]
11. Nathan TR, Whitelaw DE, Chang SC, Lees WR, Ripley PM, Payne H, Jones L, Parkinson MC, Emberton M, Gillams AR, Mundy AR, Bowen SG. Photodynamic therapy for Prostate cancer recurrence after radiotherapy: a phase I study. J. Urol. 2002; 168:1427–1432. [PubMed: 12352410]
12. Young SW, Woodburn KW, Wright M, Mody TD, Fan Q, Sessler JL, Dow WC, Miller RA. Lutetium texaphyrin (PCI-0123): a near-infrared, water-soluble photosensitizer. Photochem. Photobiol. 1996; 63:892–897. [PubMed: 8992510]
13. Mody, TD.; Fu, L.; Sessler, JL. Texaphyrins: synthesis and development of a novel class of therapeutic agents. In: Karlin, KDMody, editor. Progress in Inorg. Chem. Chichester: John Wiley and Sons Ltd; 2001. p. 551-598.
14. Stripp DC, Mick R, Zhu TC, Whittington R, Smith D, Dimofte A, Finlay JC, Miles J, Busch TM, Shin D, Kachur A, Tochner ZA, Malkowicz SB, Glatstein E, Hahn SM. Phase I trial of motexafin-lutetium-mediated interstitial photodynamic therapy in patients with locally recurrent prostate cancer. Proc. SPIE. 2004; 5315:88–99.
15. Baas P, Murrer L, Zoetmulder FAN, et al. Photodynamic therapy as adjuvant therapy in surgically treated pleural malignancies. Br. J. Cancer. 1997; 76:819–826. [PubMed: 9310252]
16. Solonenko M, Zhu TC, Vulcan T. Commissioning of the isotropic light dosimetry system for photodynamic therapy. Med. Phys. 1999; 26:1124.
17. Arnfield MR, Chapman JD, Tulip J, Fenning MC, McPhee MS. Optical properties of experimental prostate tumors in vivo. Photochem. Photobiol. 1993; 57:306–311. [PubMed: 8451295]
18. Chen Q, Wilson BC, Shetty SD, Patterson MS, Cerny JC, Hetzel FW. Changes in vivo optical properties and light distributions in normal canine prostate during photodynamic therapy. Radiat. Res. 1997; 147:86–91. [PubMed: 8989374]
19. Zhu TC, Hahn SM, Kapatkin AS, Dimofte A, Rodriguez CE, Vulcan TG, Glatstein E, Hsi RA. In vivo optical properties of normal canine prostate at 732 nm using motexafin lutetium-mediated photodynamic therapy. Photochem. Photobiol. 2003; 77:81–88. [PubMed: 12856887]

Author Manuscript Author Manuscript Author Manuscript Author Manuscript

20. Pantelides ML, Whitehurst C, Moore JV, King TA, Blacklock NJ. Photodynamic therapy for localized prostatic cancer: light penetration in the human prostate gland. J. Urol. 1990; 143:398–401. [PubMed: 2299739]
21. Whitehurst C, Pantelides ML, Moore JV, Brooman PJC, Blacklock NJ. In vivo laser light distribution in human prostatic carcinoma. J. Urol. 1994; 151:1411–1415. [PubMed: 8158797]
22. Lee LK, Whitehurst C, Pantelides ML, Moore JV. In situ comparison of 665 nm and 633 nm wavelength light penetration in the human prostate gland. Photochem. Photobiol. 1995; 62:882–886. [PubMed: 8570727]
23. Diamond KR, Patterson MS, Farrell TJ. Quantification of fluorophore concentration in tissue-simulating media by fluorescence measurements with a single optical fiber. Appl. Opt. 2003; 42:2436–2442. [PubMed: 12737480]
24. Solonenko M, Cheung R, Busch TM, Kachur A, Griffin GM, Vulcan T, Zhu TC, Wang HW, Hahn S, Yodh AG. In-vivo reflectance measurement of motexafin lutetium uptake, optical properties, and oxygenation of canine large bowels, kidneys, and prostates. Phys. Med. Biol. 2002; 47:857–873. [PubMed: 11936174]
25. Finlay JC, Zhu TC, Dimofte A, Stripp D, Malkowicz SB, Whittington R, Miles J, Glatstein E, Hahn SM. In vivo determination of the absorption and scattering spectra of the human prostate during photodynamic therapy. Proc. SPIE. 2004; 5315:132–142.
26. Doornbos RMP, Lang R, Aalders MC, Cross FW, Sterenborg HJCM. The determination of in vivo human tissue optical properties and absolute chromophore concentrations using spatially resolved steady-state diffuse reflectance spectroscopy. Phys. Med. Biol. 1999; 44:967–981. [PubMed: 10232809]
27. Kienle A, Lilge L, Patterson MS, Hibst R, Steiner R, Wilson B. Spatially resolved absolute diffuse reflectance measurements for noninvasive determination of the optical scattering and absorptions of biological tissue. Appl. Opt. 1996; 35:2304–2313. [PubMed: 21085367]
28. Jacques SL. Light Distributions from point, line and plane sources for photochemical reactions and fluorescence in turbid biological tissues. Photochem. Photobiol. 1998; 67:23–32. [PubMed: 9477762]
29. Nakai T, Nishimura G, Yamamoto K, Tamura M. Expression of optical diffusion coefficient in high-absorption turbid media. Phys. Med. Biol. 1997; 42:2541–2549. [PubMed: 9434306]
30. Storn, R.; Price, K. Global Optimiz. Vol. 11. Kluwer Academic Publishers; 1997. Differential Evolution – a simple and efficient heuristic for global optimization over continuous spacesJ; p. 341-359.
31. Zhu TC, Bjarngard BE, Ying X, Yang CJ. Modeling the output ratio in air for megavoltage photon beams. Med. Phys. 2001; 28:925–937. [PubMed: 11439489]
32. Marijnissen JPA, Star WM. Calibration of isotropic light dosimetry probes based on scattering bulbs in clear media. Phys. Med. Biol. 1996; 41:1191–1208. [PubMed: 8822784]
33. Finlay JC, Conover DL, Hull EL, Foster TH. Porphyrin bleaching and PDT-induced spectral changes are irradiance dependent in ALA-sensitized normal rat skin in vivo. Photochem. Photobiol. 2001; 73:54–63. [PubMed: 11202366]
34. Woodburn KW, Fan Q, Miles DR, Kessel D, Luo Y, Young SW. Localization and efficacy analysis of the phototherapeutic Lutetium texaphyrin (PCI-0123) in the murine EMT6 sarcoma model. Photochem. Photobiol. 1997; 65:410–415. [PubMed: 9077121]
35. Zhu TC, Dimofte A, Finlay JC, Stripp D, Busch T, Miles J, Whittington R, Malkowicz SB, Tochner Z, Glatstein E, Hahn SM. Optical properties of human prostate at 732 nm measured in vivo during motexafin lutetium-mediated photodynamic therapy. Photochem. Photobiol. 2004 in press.
36. Dimofte A, Zhu TC, Choe R-G, Hahn S. Interstitial light distribution at 730 nm prostate photodynamic therapy. Med. Phys. 2001; 28:1186.

Author Manuscript Author Manuscript Author Manuscript Author Manuscript

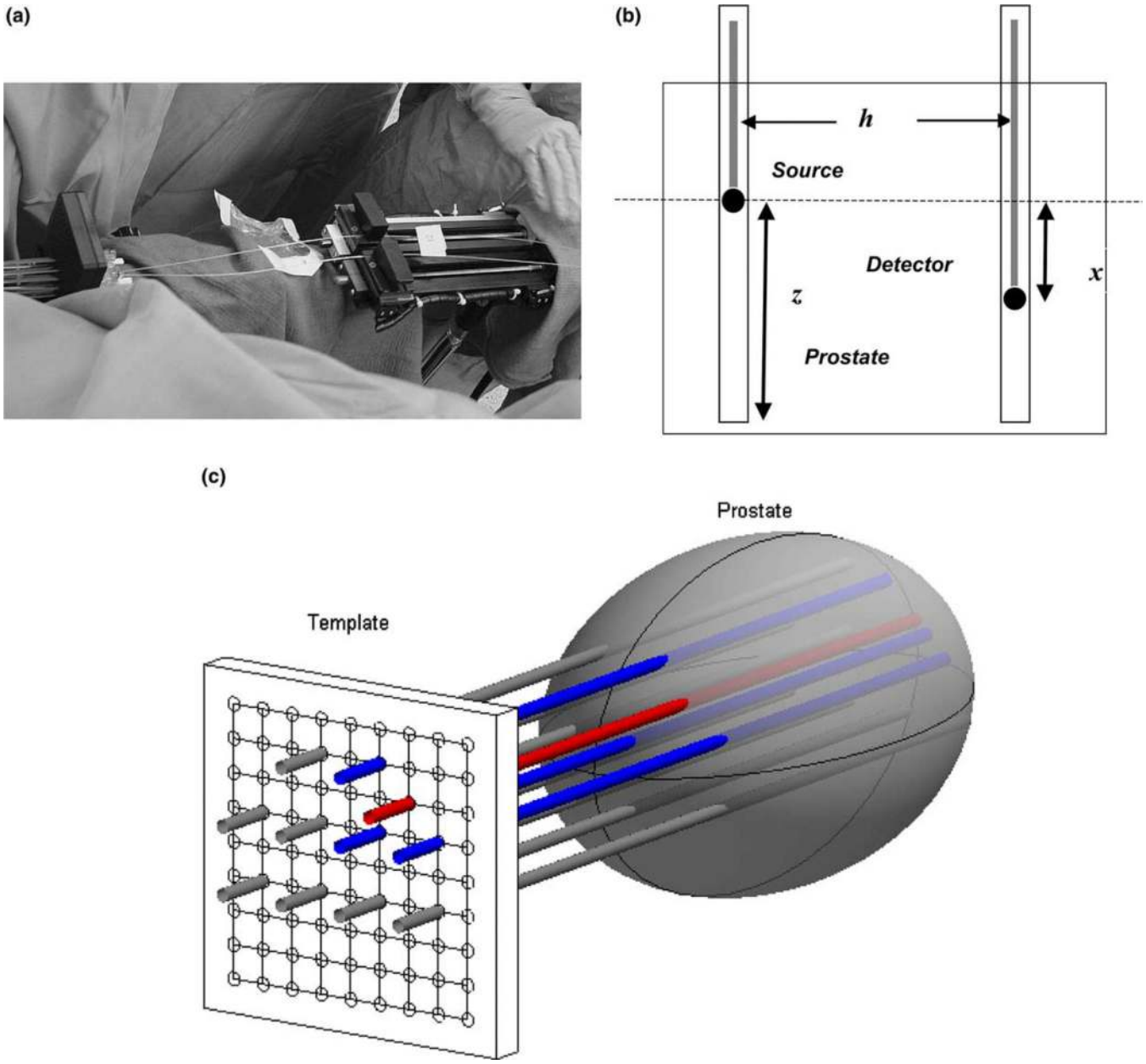

Fig. 1.

(a) Photograph and (b) Schematic of the measurement geometry, illustrating the setup for measurement of distribution of light fluence rate, optical properties, and diffuse absorption spectra. Two step motors are used, one for the light source and the other for the detector. The distribution of light fluence rate was determined by moving the detector in a catheter during initial PDT treatment. The experimental setup for the optical properties and absorption spectra measurement is identical except a different light source (732 nm vs. white light) was used. The distribution of optical properties and absorption spectra was determined by moving both a point source (by z from the end of catheter) and a detector (by x from the point source location) before and after PDT treatment. The fluorescence distribution is achieved using a single side firing fiber used as both a light source and light detector. (c) 3D

graph of the arrangement of catheters in a typical prostate treatment. The left upper quadrant's treatment (blue) and detector (red) catheters are shown in color for emphasis. The remaining catheters are for treatment of the other quadrants. The detector catheters for these quadrants are not shown.

Author Manuscript Author Manuscript Author Manuscript Author Manuscript

Author Manuscript Author Manuscript Author Manuscript Author Manuscript

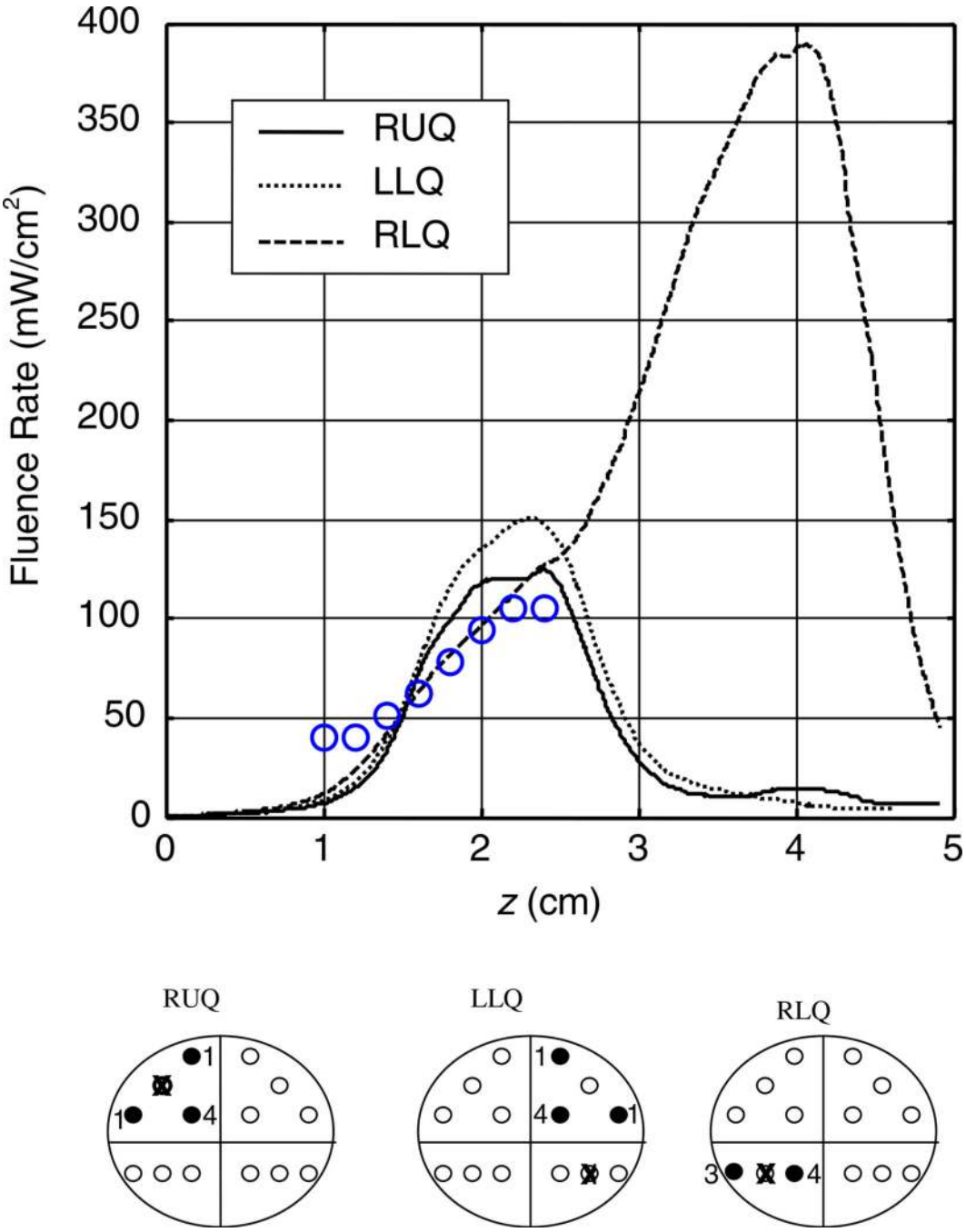

Fig. 2.

Distribution of light fluence rate for 732 nm light in-vivo during PDT. The profile measured in the LLQ was acquired during illumination of the LUQ and indicates the spread of light between adjacent quadrants. The open circles indicate the fluence rate at 0.5 cm from the source predicted by the diffusion theory using the optical properties measured at various points in the RLQ. The geometry of each measurement is shown in the diagrams below the figure. In each case, an end-view of the prostate is shown. The measurement channel in each

case is marked by an ‘x’, and the filled circles indicate the channels delivering illumination. The length in cm of the cylindrical diffuser in each channel is indicated in the diagram.

Author Manuscript Author Manuscript Author Manuscript Author Manuscript

Author Manuscript Author Manuscript Author Manuscript Author Manuscript

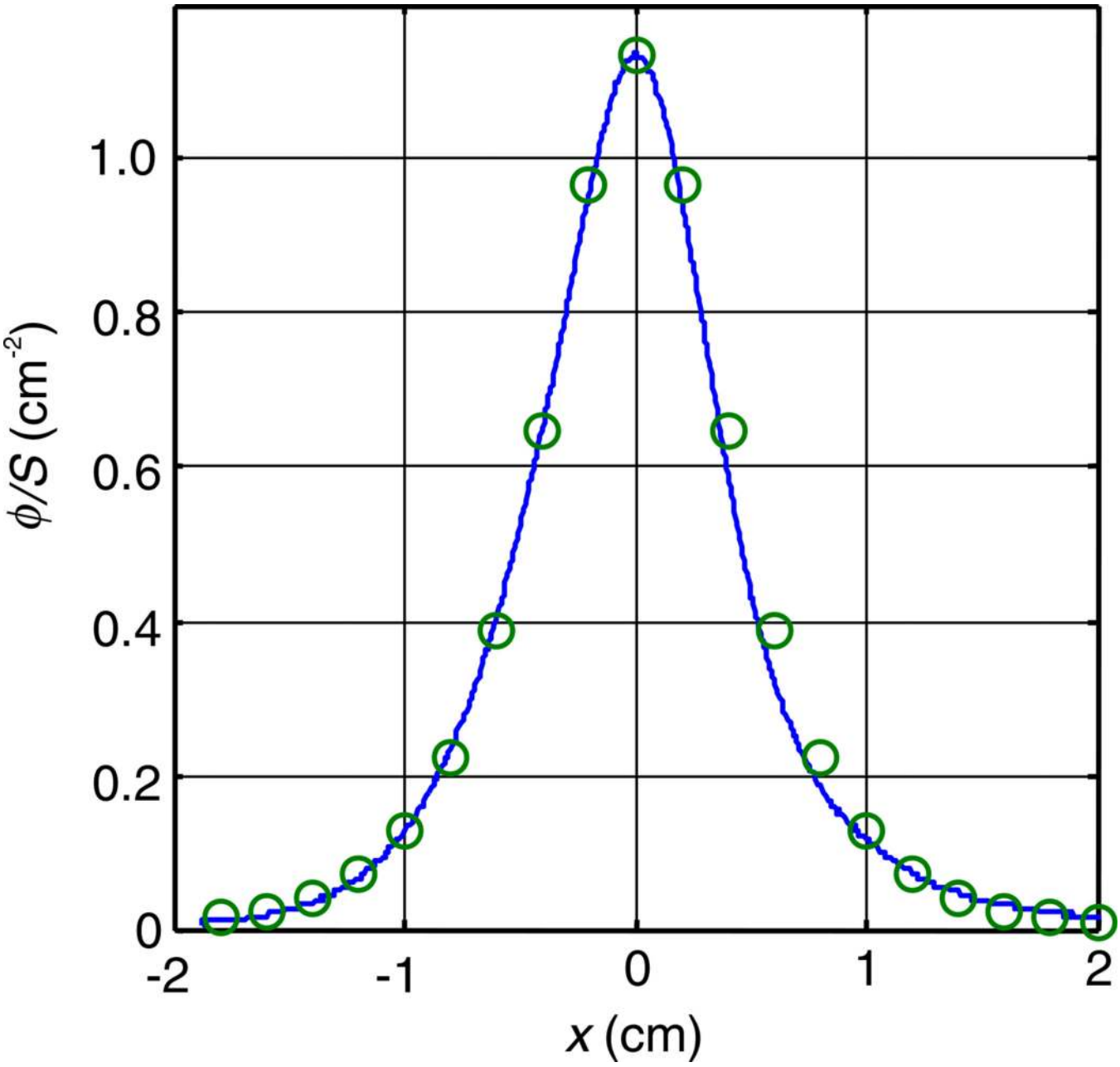

Fig. 3.

Measured light fluence rate per unit source strength (φ/S) at 732 nm versus distances along the catheter, x, from the point source measured in-vivo in human prostate gland for patient #13. Line is measured data and symbols are fits. The optical properties are: o – μ_a = 0.23 cm^{-1}, μ_s'=7.3cm^{-1}, φ(0.5)/*S* =1.1 cm^{-2}, *h* = 0.5. Similar measurements were made for different wavelengths for the absorption spectra, although the measurements are now made at only 11 points between −0.4 and 1.6 cm with 0.2 cm steps.

Author Manuscript Author Manuscript Author Manuscript Author Manuscript

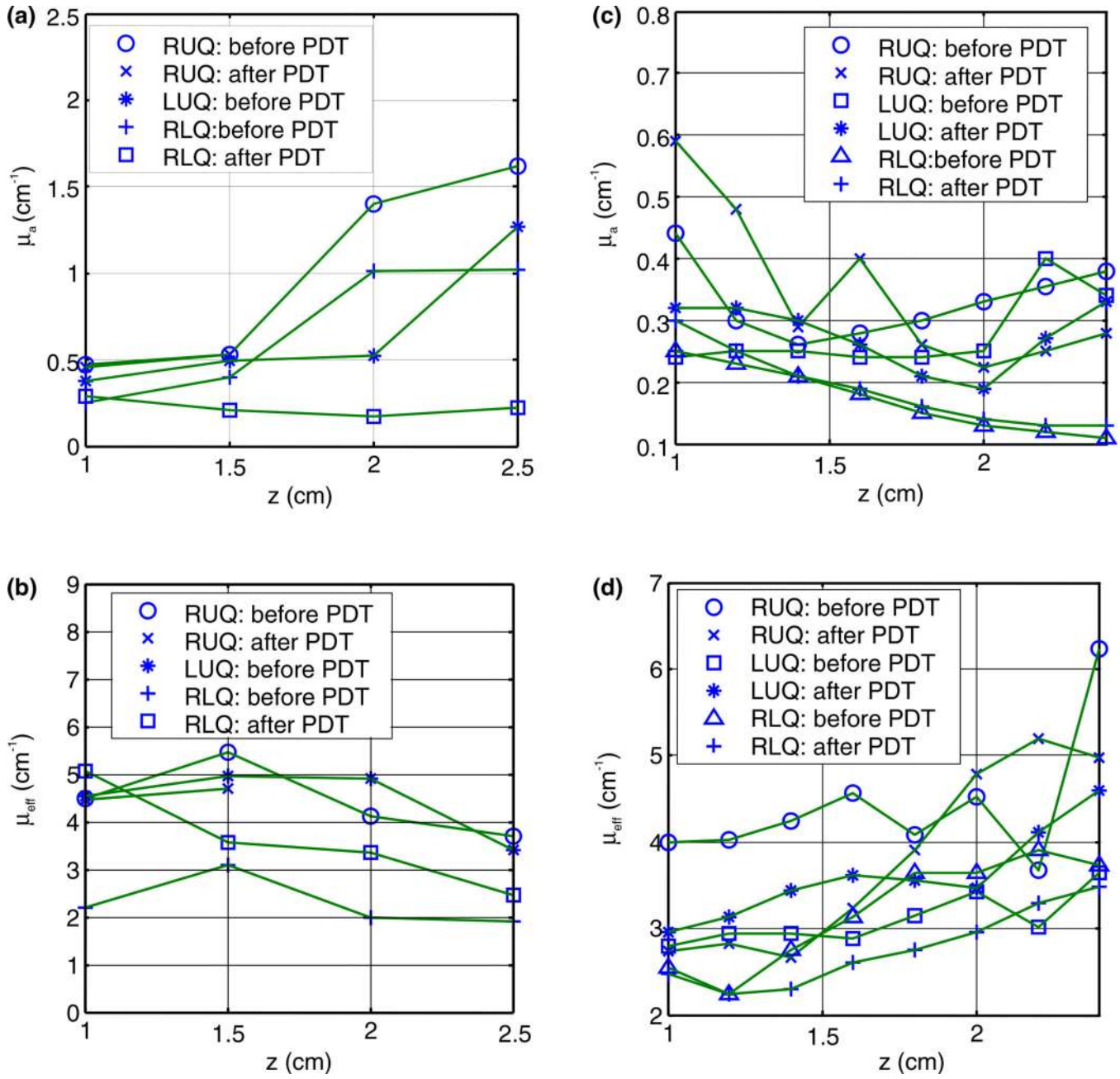

Fig. 4.

In-vivo distribution of (a) absorption and (b) effective attenuation coefficients at 732 nm in the human prostate for patient #12. (c) absorption and (d) effective attenuation coefficients at 732 nm in the human prostate for patient #13.

Author Manuscript Author Manuscript Author Manuscript Author Manuscript

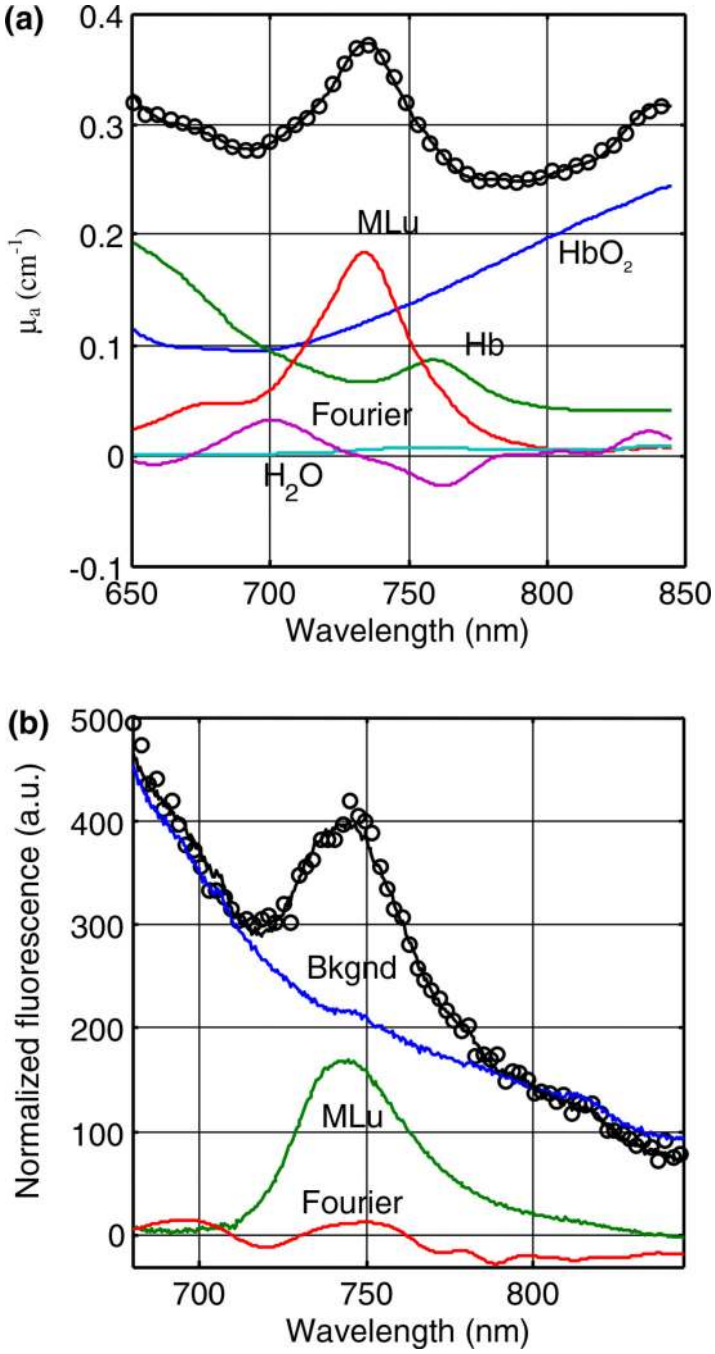

Fig. 5.

Components of (a) absorption spectra and (b) fluorescence spectra acquired prior to PDT from the LUQ of patient #13. In each case, the measured data are labeled as symbols ('o') and the components are labeled as lines. The components include: MLu, water (H_2O), deoxyhemoglobin (Hb), and hemoglobin (HbO_2). The 'Fourier' component is a Fourier series designed to account for unknown absorbers or fluorophores.

Author Manuscript Author Manuscript Author Manuscript Author Manuscript

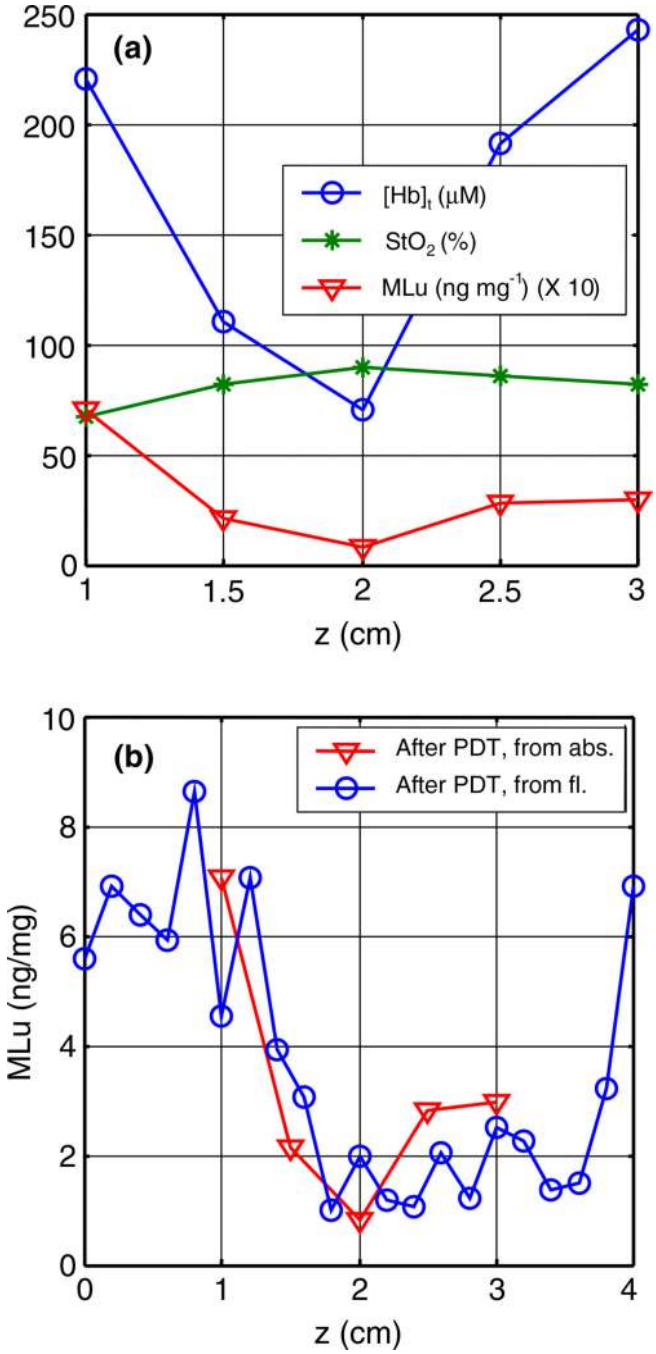

Fig. 6.

In vivo distribution of (a) StO_2, blood volume (μM), and MLu concentration determined using the absorption spectra and (b) MLu concentration as determined by absorption spectra (triangles) and fluorescence (circles) measurements for RUQ in patient 13.

Author Manuscript Author Manuscript Author Manuscript Author Manuscript

Table 1

Variation of tissue optical properties, tissue concentration of MLu, and tissue oxygenation among the two patients before and after PDT

Patient number	Light fluence (J/cm^2)	Measurement conditions	μ_a (cm^{-1})	$\mu_s' = (cm^{-1})$	μ_{eff} (cm^{-1})	MLu[a] (ng/mg)	$[Hb]_t$ (μM)	StO_2 (%)
12	50	Before PDT	0.3–1.6	1.2–18	1.9–5.4	2.5–5.0	–	–
		After PDT	0.25–0.5	5.9–39	2.5–5.0	0.4–1.7	–	–
13	100	Before PDT	0.11–0.9	7.5–40	2.2–6.3	1.4–9.2	51–310	79–88
		After PDT	0.13–0.6	5.5–34	2.2–5.2	1.1–8.1	55–370	67–89

The range specifies the minimum and maximum values of the measured quantities at different locations. Both patients received 2 mg/kg MLu intravenously at a drug-treatment interval of 3 h.

[a]For patient #12, the MLu concentration is determined from the fluorescence measurement.